Available online at www.sciencedirect.com
ScienceDirect
Advances in Space Research 40 (2007) 1281–1287
ADVANCES IN SPACE RESEARCH (a COSPAR publication)
www.elsevier.com/locate/asr

The Nuclear Compton Telescope (NCT): Scientific goals and expected sensitivity

Hsiang-Kuang Chang [a,*], Steven Boggs [b], Yuan-Hann Chang [c], for the NCT collaboration

[a] Department of Physics and Institute of Astronomy, National Tsing Hua University, Hsinchu 30013, Taiwan
[b] Department of Physics and Space Sciences Laboratory, University of California, Berkeley, CA 94720, USA
[c] Department of Physics, National Central University, Jungli 32001, Taiwan

Received 8 January 2007; received in revised form 4 July 2007; accepted 6 July 2007

Abstract

The Nuclear Compton Telescope (NCT) is a balloon-borne telescope designed to study astrophysical sources of gamma-ray emission with high spectral resolution, moderate angular resolution, and novel sensitivity to gamma-ray polarization. The heart of NCT is an array of cross-strip germanium detectors, each of 15-mm thickness and 5400 mm^2 active area, with full 3D position resolution $<2\ mm^3$. NCT will perform Compton imaging in the 0.2–10 MeV gamma-ray band. We are currently planning a 12-detector long duration balloon flight of the NCT instrument from Australia in December 2008. NCT is the prototype of a future satellite mission, which will have a coded mask on top of a larger detector array to carry out imaging in the 20–100 keV X-ray band. This paper describes the scientific goals, as well as the detector design, simulated performance and current status of the project. NCT is a joint effort of several institutions in the US and in Taiwan.
© 2007 COSPAR. Published by Elsevier Ltd. All rights reserved.

Keyword: Gamma-ray telescopes and instrumentation

1. Introduction

Soft gamma-ray (0.2–10 MeV) astronomy is undergoing a technological revolution through the development of large-volume, high spectral and spatial resolution tracking detectors, such as the 3D-positioning germanium detectors (3D-GeDs) developed in the Nuclear Compton Telescope (NCT) project. Building upon the Compton imaging technique pioneered by COMPTEL on CGRO (Schönfelder et al., 1993), the 3D positioning enables a much more compact telescope design. Tracking technologies provide dramatic improvements in Compton efficiency and sensitivity. The Nuclear Compton Telescope (NCT) is a balloon-borne soft gamma-ray telescope designed to study astrophysical sources of nuclear line emission and gamma-ray polarization. It employs a novel Compton telescope design utilizing twelve 3D-GeDs with high spectral and spatial resolution to track gamma-ray Compton-scattering interactions (Fig. 1 and Table 1). Compton tracking serves three purposes: imaging the sky, measuring polarization, and reducing background. The array, enclosed on the sides and bottom by an active BGO well, is collimated to a field-of-view (FOV) of $40° \times 60°$ FWHM. The telescope will be mounted in a pointed, autonomous long-duration balloon flight (LDBF) platform, planned to fly from Australia in end 2008. In the following sections we describe some of the major scientific goals, detector design, and expected sensitivity of the current NCT project. Previous reports on NCT can be found in Boggs et al. (2003, 2004) and Coburn et al. (2005).

NCT has two main advantages over INTEGRAL/SPI for the nuclear science studies described here. First, Compton imaging does not suffer from insensitivity to large-scale diffuse emission like the coded-aperture imaging used on SPI. And second, NCT's sensitivity is not nearly as background-limited. At its limiting sensitivity NCT has a back-

* Corresponding author. Tel.: +886 3 5742952; fax: +886 3 5723052.
E-mail address: hkchang@phys.nthu.edu.tw (H.-K. Chang).

0273-1177/$30 © 2007 COSPAR. Published by Elsevier Ltd. All rights reserved.
doi:10.1016/j.asr.2007.07.012

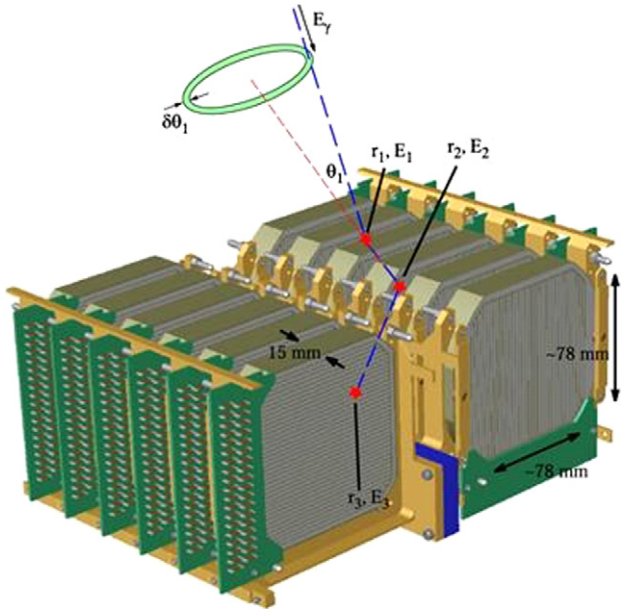

Fig. 1. The heart of NCT, an array of 12 cross-strip GeDs with 3D tracking resolution. By measuring the position and energy of each photon interaction, the initial photon direction can be determined to within an annulus (event circle) on the sky.

Table 1
NCT performance (3 σ, 800 ks)

Energy range	0.2–10 MeV
Spectral resolution	0.2–1% FWHM
Field of view (FoV)	$40° \times 60°$ FWHM
Angular resolution	~2°–3° HPHW
Effective area	5–18 cm^2
Narrow line sensitivity	$(1–2) \times 10^{-5}$ photons cm^{-2} s^{-1}
Continuum sensitivity	$\sim 1/E(\text{MeV}) \times 10^{-4}$ photons cm^{-2} s^{-1} MeV^{-1}
100% polarization sensitivity	37 m Crab (0.2–0.5 MeV)

ground-to-source ratio <10, while SPI has a ratio roughly 500:1. This enables NCT to explore a new phase space of gamma-ray observations.

2. Major scientific goals

2.1. The galactic electron–positron annihilation line emission

Production of positrons and their annihilation in the galactic interstellar medium (ISM) is one of the pioneering topics of gamma-ray astronomy. After three decades of observations, however, the origin of these positrons remains a mystery. The leading theory is that positrons are predominantly created in the β^+-decay of radioisotopes produced in SNe Ia (Milne et al., 1999). However, INTEGRAL observations of SN 1006 have ruled out SNe Ia as the sole source of positrons, without constraining their actual contribution (Kalemci et al., 2006). Observations made by the CGRO/OSSE and INTEGRAL/SPI instruments support a time-invariant emission that features an anomalously large contribution from the galactic bulge/halo, relative to emission at other wavelengths (Purcell et al., 1997; Knödlseder et al., 2005; Jean et al., 2006). As it becomes increasingly clear that the emission is brightest in the direction of the galactic center, but that the emission appears truly diffuse (rather than from a point source near the galactic center), new theories are being explored to explain the bulge/halo positrons. Potential sources include SNe Ia (Milne et al., 1999), hypernovae from an episode of starburst activity in the bulge (Cassé et al., 2004; Parizot et al., 2005), star-capture by the central black hole (Cheng et al., 2006), electron–positron pairs from millisecond pulsars (Wang et al., 2006), and annihilations or decays of (as yet undiscovered) light dark matter particles (Boehm et al., 2004, 2005). Mapping the spatial distribution of this emission remains a crucial key to understanding the origin of the positrons.

NCT will map the galactic central radian 0.511-MeV distribution with high S/N ratio and a 3° resolution. With the combined maps and spectral widths, we will investigate the galactic positron sources and annihilation sites in detail. The sensitivity and ability to map large-scale emission, as well as its wider FOV for uniform galactic center exposure, gives NCT major advantages over SPI for these studies.

2.2. Origins of ^{26}Al

COMPTEL mapped the galactic plane 1.809 MeV emission with 3.8° FWHM angular resolution (Oberlack et al., 1996), revealing hotspots potentially associated with our galaxy's spiral arms, the Cygnus region, the Vela SNR, and OB associations. INTEGRAL/SPI has recently published the first resolved spectroscopy of this emission, verifying the galaxy-wide distribution through measurement of the galactic rotational broadening of the line (Diehl et al., 2006). ^{26}Al has a half-life of 7.2×10^5 years, and decays to ^{26}Mg, emitting a characteristic 1.809 MeV photon. The integrated 1.809 MeV flux is widely believed to map core-collapse SNe activity in our Galaxy over the last 10^6 years, corresponding to $\sim 10^4$ combined SNe. Other potential sources of ^{26}Al include Wolf–Rayet (W–R) stars, AGB stars, and classical novae (Diehl and Timmes, 1998, and references therein); however, the COMPTEL map rules out novae and AGB stars as a significant source of ^{26}Al (Knödlseder et al., 1999).

A key measurement to determine the origin of ^{26}Al will be the detection of ^{60}Fe emission. Once produced, ^{60}Fe decays to ^{60}Co with a half-life of 1.5×10^6 years, which rapidly decays to ^{60}Ni emitting two gamma-ray photons, 1.173 and 1.333 MeV. The production of ^{60}Fe in W–R stars is negligible, while in core-collapse SNe ^{60}Fe production is ~40% of the ^{26}Al production (Prantzos, 2004). The ^{60}Fe lines should follow the 1.809 MeV line at about 11–16% the flux for nuclei produced in core-collapse SNe. Ten instruments have measured ^{26}Al emission from the galactic center region, all of which are consistent with a flux of

4×10^{-4} photons $cm^{-2}\,s^{-1}\,rad^{-1}$ for the central radian (Diehl and Timmes, 1998). Recent RHESSI and SPI detections have placed limits on the $^{60}Fe/^{26}Al$ flux ratio of $11 \pm 3\%$ (Harris et al., 2005), marginally excluding core collapse SNe as the sole source. The GRIS experiment also measured a surprisingly broad 1.809 MeV line width of 5.4 ± 1.3 keV (Naya et al., 1998). However, both RHESSI and SPI measured a narrower width with better statistics, which is consistent with the expected broadening due only to galactic rotation (Smith, 2003; Diehl et al., 2006). For an 800-ks NCT/LDBF observation of the integrated ^{26}Al and ^{60}Fe emission from the central galactic radian, assuming the 11% flux ratio, the signal-to-noise (S/N) ratio for the extended ^{26}Al is 36 σ, while the combined S/N ratio in the two ^{60}Fe lines is 5–6 σ (if distributed similar to ^{26}Al). NCT will map the ^{26}Al distribution, spatially resolving the 1.809 MeV line position and width along the galactic plane. NCT will also make the first crude map of the ^{60}Fe emission, while measuring the the $^{60}Fe/^{26}Al$ flux ratio. NCT has two major advantages over SPI for these studies – higher sensitivity, and the fact that Compton imaging is inherently more sensitive to diffuse emission than coded-aperture imaging.

2.3. Gamma-ray pulsars

Among about 1500 catalogued radio pulsars, seven are found to emit gamma rays with pulsations at their radio periods, and three more are detected with relatively lower confidence levels (e.g., Thompson, 2003). There is still no consensus on how pulsars manage to emit these gamma rays, particularly regarding the emission site and mechanisms, although the number of observed gamma-ray pulsars will increase dramatically soon after the launch of AGILE and GLAST. Models of gamma-ray emission from pulsars have long divided themselves into two broad categories: the polar-cap models (e.g., Zhang and Harding, 2000) and the outer-gap models (e.g., Cheng et al., 2000). The main difference between these two groups of models, among others, is the location in the magnetosphere where the observed gamma rays are emitted. In the polar-cap models, the emission site is close to the star, while in the outer-gap models it is in the outer magnetosphere of the pulsar. Recently, the slot-gap concept (Arons, 1983) has been incorporated into the polar-cap model, which allows an emission site at a higher altitude in the inner magnetosphere of the pulsar (Muslimov and Harding, 2003). A stationary pair production cascade in outer magnetospheres was studied in Hirotani et al. (2003), in which the inner boundary of the outer gap is shifted from the null surface inward towards the stellar surface. In a similar study, the two-dimensional outer-gap structure was investigated with the Monte Carlo technique (Takata et al., 2006).

One important characteristic potentially crucial for discriminating these models is their prediction of the polarization patterns. Polarization measurement of radio emission has been a routine work for pulsars, but for higher energy emissions the only measurement is the optical polarization of the Crab pulsar (Smith et al., 1988; Kanbach et al., 2003). Based on the optical measurement, the X-ray polarization of the Crab pulsar has been predicted with different models (Chen et al., 1996; Dyks et al., 2004; Takata et al., 2007). Theoretical prediction of the MeV polarization of the Crab pulsar will be reported in a forthcoming paper. NCT may be able to measure the MeV polarization of the Crab pulsar or to place an upper limit to that.

3. The instrument

The NCT is an array of twelve 3D-GeD gamma-ray Compton-tracking detectors (Fig. 1). The 3D-GeD array is housed in a common cryostat, which is enclosed on the sides and bottom by a 5-cm thick active BGO anticoincidence shield, and collimated to $40^\circ \times 60^\circ$ by 5-cm Pb bricks surrounded by an active plastic shield. NCT has a large FOV, and is mounted in an autonomous LDBF platform designed for full-sky elevation and azimuthal pointing.

3.1. The detector

The NCT detectors are custom 15-mm thick cross-strip GeDs of active area 5400 mm^2 each. Orthogonal 37×37 2-mm pitch electrode strips on the opposite faces, combined with signal timing, provide full 3D position resolution to 1.6 mm^3. A gap of 0.25 mm between the strips for the 2.0 mm pitch has been demonstrated by LBNL to minimize the number of charge sharing events and the resulting charge loss, while maintaining the high GeD spectral resolution. A 2-mm thick guard ring surrounds this active area on both faces of the detector, with a 1-mm gap between the ring and the edge of the crystal. The guard rings are instrumented to provide anticoincidence signals for rejection of events with interactions in these regions. The NCT 3D-GeDs operate as fully depleted p-i-n junctions, using amorphous Ge contact technologies pioneered by LBNL (Luke et al., 1992). In this technique, the blocking electrode is made from a ~0.1-μm thick layer of amorphous Ge deposited on the entire detector surface. The strip electrodes are defined by evaporating a layer of metal through a shadow mask on top of the amorphous Ge film. This amorphous film serves as the blocking contact, and fully passivates every detector surface not used for contact connection. The bipolar blocking behavior of the amorphous contacts allows them to be used on both sides of the detector, replacing the conventional n-type lithium contact and p-type ion implanted contact. The amorphous germanium can be made highly resistive which provides excellent inter-electrode impedance (Luke et al., 1994), which has been demonstrated to significantly improve the charge collection for events that occur in the inter-strip region, and allows for excellent spectroscopy even when charge is shared by neighboring strips (Amman and Luke, 2000). The amorphous contact fabrication has proven reliable, providing high yields of successful detectors. Only a

few simple steps are involved in the manufacturing process. The amorphous contacts are also robust. Our first prototype strip detector operated successfully for over 5 years with no measurable degradation of the performance. In addition, the contacts have been shown to be stable with temperature up to 100 °C for more than 12 h, which will permit detector annealing for radiation damage repair in future satellite applications.

3.2. Performance simulation

Given the complexity of gamma-ray photon interactions, which include Compton scattering, photo-absorption, and pair production as well as complex backgrounds produced by diffuse photons, cosmic rays and secondary neutrons, only Monte Carlo simulations including all background components followed by full Compton data analysis of all sources and backgrounds can reliably estimate the performance of any Compton telescope. One of NCT's primary goals is to verify both instrument performance predictions and background simulations of modern high-resolution Compton telescope designs in realistic radiation environments. The expected performance of NCT was predicted using the full ACT simulation toolset (based on MGGPOD (Weidenspointner et al., 2005) and MEGAlib (Zoglauer et al., 2006)). The simulated background environment includes an atmospheric gamma-ray input spectrum based on the anisotropic gamma-ray distribution from Gehrels (1985), atmospheric neutrons from Armstrong et al. (1973), corrected for the Australian LDBF altitude and latitude, and cosmic-ray protons and electrons from Mizuno et al. (2004), corrected for the effective cutoff rigidity at the balloon latitude for solar minimum. In addition, the most prominent atmospheric line, the 511 keV annihilation line, was scaled from Harris et al. (2003) Our simulations include a realistic model of the balloon gondola, the detector, Great care has been taken to accurately include all passive materials close to the detector. Detector position and energy resolution were faithfully represented in the simulation: deposited energies were randomly modified to reflect the energy resolution measured by calibrations, and positions were discretized according to the strip pitch of the GeD. Interactions spanning several channels (charge sharing) are combined, with a detector threshold of 15 keV (40 keV trigger threshold) corresponding to NCT's current performance.

3.3. Instrument backgrounds

In Fig. 2 we show our background simulations for the NCT 2005 prototype flight (Coburn et al., 2005), compared with our simulated background. This plot shows the background of all photon events that Compton scattered between the two detectors in the prototype, no imaging applied, which is the easiest and most robust way of comparing the measured and simulated backgrounds for Compton-scattering events. As can be seen in this figure,

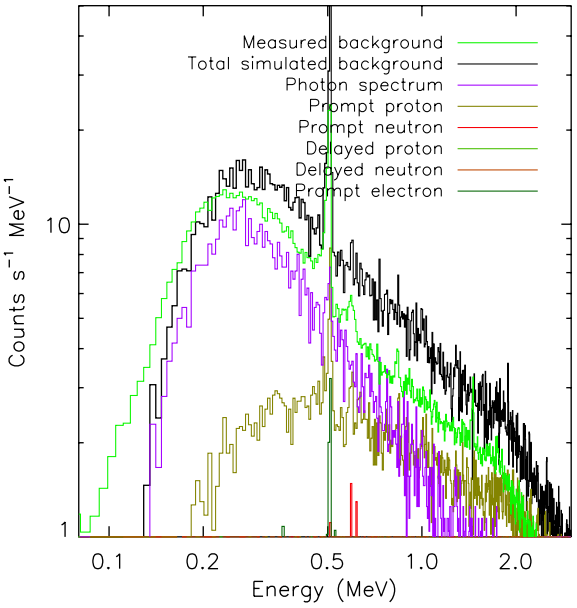

Fig. 2. Comparison of the NCT prototype background measurements with the expectations from simulations. These are all photons scattered between the two prototype detectors, with no imaging applied. The NCT background is dominated by atmospheric photons, which is consistent with the low number of background lines (with the exception of the atmospheric positron annihilation) compared with most germanium instruments. The delayed neutron and prompt electron components of the background fall below the scale of this plot, but were included in the simulations. The simulation was performed by J. Bowen et al.

our measured backgrounds are significantly lower in the primary energy band of NCT, 0.2–2 MeV, than the simulations predict, as low as 60%. However, we can see from the simulations that the dominant background component for NCT is atmospheric photons. As noted above, for our background simulations we take the conservative Gehrels (1985) spectra and angular distribution. However, there is a large uncertainty in this photon component, as demonstrated by the spectrum of the downward photons from Dean et al. (1991), which has roughly a factor 2 lower in flux than the Gehrels (1985) spectrum, and is more consistent with the NCT prototype observations. Given the historical uncertainty in this component, however, we have included a range of values for our sensitivity estimates, based on both the simulations including the more conservative Gehrels (1985) photon spectrum, and estimates scaled to our measured NCT prototype backgrounds.

3.4. Effective area

In Fig. 3 we show our simulated on-axis effective area for all photopeak events which are properly Compton imaged back to the source position, and are not vetoed by any of our event cuts used to reduce background. Hence, this is the actual effective area required to determine the instrumental sensitivity. (The non-imaging photopeak effective area would be higher, but not all of those events would be properly imaged or accepted by the event cut criteria.)

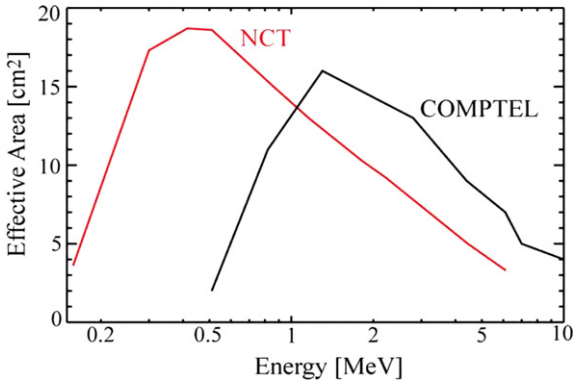

Fig. 3. On-axis photopeak effective area (before atmospheric attenuation). COMPTEL is shown for comparison (Schönfelder et al., 1993). NCT has less than 1% of the COMPTEL detector volume.

3.5. Angular resolution measure

NCT's compact design enables wide-field imaging capabilities. Angular resolution in Compton telescopes is described in terms of the angular resolution measure (ARM), defined as the smallest distance of the reconstructed Compton cone to the true source direction. The half-power half-width (HPHW) of the on-axis ARM distribution as a function of energy is shown in Fig. 4. Position resolution of the individual interactions dominates the angular resolution below ~2 MeV. At higher energies, the angular resolution is dominated by the degradation in the spatial resolution due to the increased electron range.

3.6. Sensitivity

The narrow line (Fig. 5), continuum (Fig. 6), and polarization (Fig. 7) sensitivities for an on-axis source were calculated including standard source and background statistics (Jean et al., 1996; Lei et al., 1997). We have included all source and background photons whose event circles cross within ~2× the energy-dependent ARM distance from the assumed source position. We have included an estimated sensitivity range, based

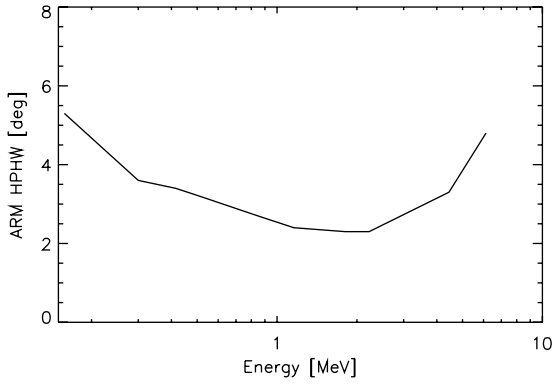

Fig. 4. The simulated on-axis angular resolution measure (ARM) for NCT.

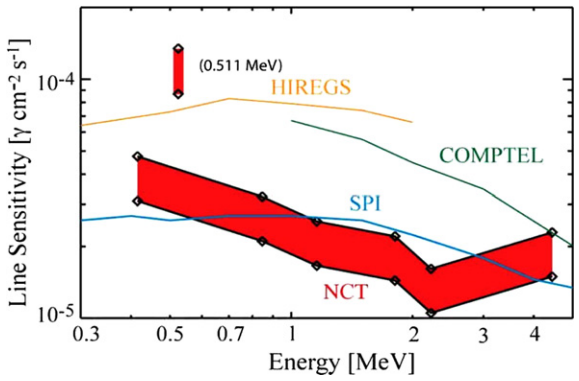

Fig. 5. Narrow line sensitivity (3 σ) for 800 ks observing time compared with COMPTEL, SPI, and the HIREGS LDBF mission. The ~ 40% uncertainty range is based on the a priori background simulation (more conservative) and our measured background on the prototype flight in June 2005 (more optimistic). Our measured background was roughly a factor 2.4 lower than simulations.

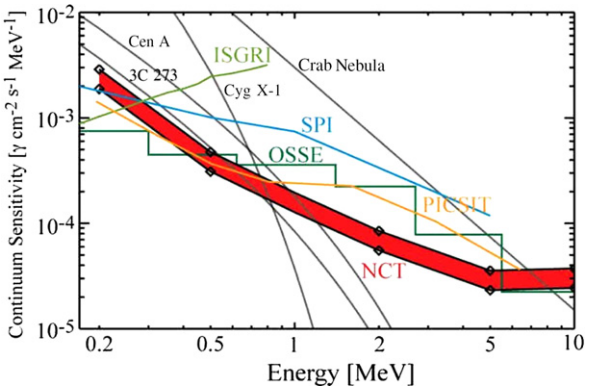

Fig. 6. Continuum sensitivity (3 σ, $\Delta E = E$) for an 800-ks observation. The extrapolated spectra of several sources are shown for comparison. INTEGRAL sensitivities are derived from the AO4 Observer's manual.

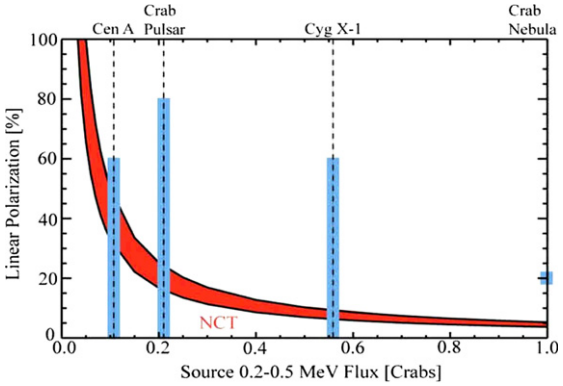

Fig. 7. Fractional linear polarization sensitivity (3 σ, 800 ks) as a function of 0.2–0.5 MeV flux. Shown for comparison are the ranges of predicted/expected polarizations for few sources.

both on backgrounds from our current simulations and on backgrounds scaled to agree with our prototype flight measurements. We have not accounted for instrument dead times when processing photon or charged particle

events, or when the shields have been triggered. However, the measured NCT prototype dead time during flight was less than 8% (which is typical of measured dead times for shielded spectrometers flying at mid-latitudes, e.g. HEXAGONE), which will affect the sensitivity by less than 4%. The sensitivities are shown for an 800-ks observation.

4. Summary

NCT utilizes an array of cross-strip 3D-tracking GeDs to perform Compton imaging and spectrometry. It is a relatively small instrument, and yet achieves Compton-imaging effective areas comparable to COMPTEL (Fig. 3), with significantly improved sensitivity (Figs. 5–7). Scientific goals of the current NCT project with a 12-GeD array include, but not limited to, the galactic electron–positron annihilation line emission, the origins of ^{26}Al, and gamma-ray pulsars. An NCT LDBF is planned in end 2008. A possible future small-satellite mission carrying a larger array of GeDs with a coded mask to cover the hard X-ray band is being discussed. The NCT project is funded by NASA under Grant #NNG04WC38G for the NCT-US team and by the National Space Organization (NSPO) in Taiwan under Grant 95-NSPO(B)-SP-FA04-01 for the NCT-Taiwan team.

References

Amman, M., Luke, P.N. Three-dimensional position sensing and field shaping in orthogonal-strip germanium gamma-ray detectors. NIM A452, 155–166, 2000.

Armstrong, T.W., Chandler, K.C., Barish, J. Calculations of neutron flux spectra induced in the Earth's atmosphere by galatic cosmic rays. J. Geophys. Res. 78, 2715–2726, 1973.

Arons, J. Pair creation above pulsar polar caps – geometrical structure and energetics of slot gaps. ApJ 266, 215–241, 1983.

Beacom, J.F., Bell, N.F., Bertone, G. Gamma-ray constraint on galactic positron production by MeV dark matter. PRL 94, 171301, 2005.

Boehm, C., Hooper, D., Silk, J., et al. MeV dark matter: has it been detected? PRL 92, 101301, 2004.

Boggs, S.E., Amrose, S., Coburn, W., et al. Upcoming balloon flight of the Nuclear Compton Telescope. SPIE 4851, 1221–1227, 2003.

Boggs, S.E., Coburn, W., Smith, D.M., et al. Overview of the Nuclear Compton Telescope. New Astr. Rev. 48, 251–255, 2004.

Cassé, M., Cordier, B., Paul, J., Schanne, S. Hypernova/gamma-ray bursts in the galactic center as possible sources of galactic positrons. ApJ 602, L17–L20, 2004.

Chen, K., Chang, H.-K., Ho, C. Optical pulse polarization of the Crab pulsar. ApJ 471, 967–972, 1996.

Cheng, K.S., Chernyshov, D.O., Dogiel, V.A. Annihilation emission from the galactic black hole. ApJ 645, 1138–1151, 2006.

Cheng, K.S., Ruderman, M., Zhang, L. A three-dimensional outer magnetospheric gap model for gamma-ray pulsars: geometry, pair production, emission morphologies, and phase-resolved spectra. ApJ 537, 964–976, 2000.

Coburn, W., Boggs, S.E., Bowen, J.D., et al. First results from the balloon flight of the NCT prototype. SPIE 5898, 13–21, 2005.

Dean, A.J., Lei, F., Knight, P.J. Background in space-borne low-energy gamma-ray telescopes. Space Sci. Rev. 57, 109–186, 1991.

Diehl, R., Halloin, H., Kretschmer, K., et al. Radioactive ^{26}Al from massive stars in the Galaxy. Nature 439, 45–47, 2006.

Diehl, R., Timmes, F.X. Gamma-ray line emission from radioactive isotopes in stars and galaxies. PASP 110, 637–659, 1998.

Dyks, J., Harding, A.K., Rudak, B. Relativistic effects and polarization in three high-energy pulsar models. ApJ 606, 1125–1142, 2004.

Gehrels, N. Instrumental background in balloon-borne gamma-ray spectrometers and techniques for its reduction. NIM A239, 324–349, 1985.

Harris, M.J., Share, G.H., Leising, M.D. Spatial and temporal variability of the gamma radiation from Earth's atmosphere during a solar cycle. JGR 108, 1435, 2003.

Harris, M.J., Knödlseder, J., Jean, P., et al. Detection of gamma-ray lines from interstellar Fe-60 by the high resolution spectrometer SPI. A&A 433, L49–L52, 2005.

Hirotani, K., Harding, A.K., Shibata, S. Electrodynamics of an outer gap accelerator: Formation of a soft power-law spectrum between 100 MeV and 3 GeV. ApJ 591, 334–353, 2003.

Jean, P., Naya, J.E., Olive, J.F., et al. Instrument concepts for high resolution gamma-ray spectroscopy. A&AS 120, C673–C676, 1996.

Jean, P., Knödlseder, J., Gillard, W., Guessoum, N., Ferriére, K., Marcowith, A., Lonjou, V., Roques, J.P. Spectral analysis of the Galactic e^+e^- annihilation emission. A&A 445, 579–589, 2006.

Kalemci, E., Boggs, S.E., Milne, P.A., Reynolds, S.P. Searching for annihilation radiation from SN 1006 with SPI on INTEGRAL. ApJ 640, L55–L57, 2006.

Kanbach, G., Kellner, S., Schrey, F.Z., et al. Design and results of the fast timing photo-polarimeter OPTIMA. SPIE 4841, 82–93, 2003.

Knödlseder, J., Bennett, K., Bloemen, H., et al. A multiwavelength comparison of COMPTEL 1.8 MeV Al-26 line data. A&A 344, 68–82, 1999.

Knödlseder, J., Jean, P., Lonjou, V., et al. The all-sky distribution of 511 keV electron–positron annihilation emission. A&A 441, 513–532, 2005.

Lei, F., Dean, A.J., Hills, G.L. Compton polarimetry in gamma-ray astronomy. Space Sci. Rev. 82, 309–388, 1997.

Luke, P.N., Cork, C.P., Madden, N.W., et al. Amorphous Ge bipolar blocking contacts on Ge detectors. IEEE Transact. Nucl. Sci. 39, 590–594, 1992.

Luke, P.N., Pehl, R.H., Dilmanian, F.A. A 140-element Ge detector fabricated with amorphous Ge blocking contacts. IEEE Transact. Nucl. Sci. 41, 976–978, 1994.

Milne, P.A., The, L.S., Leising, M.D. Positron escape from type Ia supernovae. ApJS 124, 503–526, 1999.

Mizuno, T., Kamae, T., Godfrey, G., et al. Cosmic-ray background flux model based on a Gamma-Ray Large Area Space Telescope balloon flight engineering model. ApJ 614, 1113–1123, 2004.

Muslimov, A.G., Harding, A.K. Extended acceleration in slot gaps and pulsar high-energy emission. ApJ 588, 430–440, 2003.

Naya, J.E., Barthelmy, S.D., Bartlett, L.M., et al. Gamma-ray limits on galactic Fe-60 nucleosynthesis and implications on the origin of the Al-26 emission. ApJ 499, L169–L173, 1998.

Oberlack, U., Bennett, K., Bloemen, H., et al. The COMPTEL 1.809 MeV all-sky image. A&AS 120, C311–C314, 1996.

Parizot, E., Cassé, M., Lehoucq, R., Paul, J. GRBs and the 511 keV emission of the Galactic buldge. A&A 432, 889–894, 2005.

Prantzos, N. Radioactive ^{26}Al and ^{60}Fe in the Milky Way: implications of the RHESSI detection of ^{60}Fe. A&A 420, 1033–1037, 2004.

Purcell, W.R., Cheng, L.X., Dixon, D.D., et al. OSSE mapping of galactic 511 keV positron annihilation line emission. ApJ 491, 725–748, 1997.

Schönfelder, V., Aarts, H., Bennet, K., et al. Instrument description and performance of the imaging gamma-ray telescope COMPTEL aboard the Compton Gamma-Ray Observatory. ApJS 86, 657–692, 1993.

Smith, D.M. The Reuven Ramaty High Energy Solar Spectroscopic Imager observation of the 1809 keV line from galactic ^{26}Al. ApJ 589, L55–L58, 2003.

Smith, F.G., Jones, D.H.P., Dick, J.S.B., et al. The optical polarization of the Crab pulsar. MNRAS 233, 305–319, 1988.

Takata, J., Shibata, S., Hirotani, K., Chang, H.-K. A two-dimensional electrodynamical outer gap model for gamma-ray pulsars: gamma-ray spectrum. MNRAS 366, 1310–1328, 2006.

Takata, J., Chang, H.-K., Cheng, K.S. Polarization of high-energy emissions from the Crab pulsar. ApJ 656, 1044–1055, 2007.

Thompson, D.J., Gamma ray pulsars – Multiwavelength observations. Available from: astro-ph/0312272, 2003

Wang, W., Pun, C.S.J., Cheng, K.S. Could electron–positron annihilation lines in the galactic center result from pulsar winds? A&A 446, 943–948, 2006.

Weidenspointner, G., Harris, M.J., Sturner, S., et al. MGGPOD: a Monte Carlo suite for modeling instrumental line and continuum backgrounds in gamma-ray astronomy. ApJS 156, 69–91, 2005.

Zhang, B., Harding, A.K. Full polar cap cascade scenario: gamma-ray and X-ray luminosities from spin-powered pulsars. ApJ 532, 1150–1171, 2000.

Zoglauer, A., Andritschke, R., Schopper, F. MEGAlib – The medium energy gamma-ray astronomy library. New Astr. Rev. 50, 629–632, 2006.